On-Body Low-Profile Textile Antenna with Artificial Magnetic Conductor

Ala Alemaryeen, *Student Member, IEEE,* and Sima Noghanian, *Senior Member, IEEE*

***Abstract*—A compact low-profile wearable antenna is proposed. The antenna is a combination of monopole with an artificial magnetic conductor (AMC) as a ground plane. The proposed AMC integrated antenna is fabricated using layers of textile and is operating within the industrial, scientific, and medical ISM 5.8 GHz band. The proposed low-profile AMC antenna features a small footprint, with dimensions of 102 × 68 × 3.6 mm^3, and yields an impedance bandwidth of 34% (4.30 GHz – 5.90 GHz), with a gain value of 6.12 dBi. Numerical and experimental investigations reveal that the performance of the proposed integrated AMC antenna is robust with respect to structural deformations, i.e., bending and crumpling, as well as human body loading, and shows superior performance to the conventional monopole antenna. Additionally, numerical investigations indicate that the inclusion of the AMC structure considerably reduces the specific absorption rate (SAR) values for different planer and bending scenarios. For on body analysis, three different body models of different compositions and shapes were used. Also experiments were performed utilizing body phantoms. The proposed AMC antenna is a promising candidate for wearable wireless devices.**

***Index Terms*—Metamaterials, specific absorption rate (SAR), textile antennas, wearable antennas.**

I. Introduction

WEARABLE electronic systems have attracted increasing interests due to their potential applications in a wide variety of fields including medical care, health-monitoring, patient-tracking, and emergency rescue operations. As an important component of these wearable systems, the antenna plays a vital role for the wireless communication between the on-body sensors and other on-/off-body devices [1]-[2]. Because wearable antennas operate in close proximity of the human body, antenna engineers should consider many potential factors in the initial stages of the design. Hence, the design process of a wearable flexible antenna is quite different compared to the design of traditional antennas that are not normally working in the vicinity of human body.

First, the electromagnetic coupling to the human body should be studied because it may influence antenna's performance, i.e., frequency detuning and radiation degradation, due to the lossy nature of human tissues [3]. In addition, electromagnetic power absorbed by the body may pose potential health risks, especially if a long-term irradiation to the human body exists. Hence, in order for wearable antennas to adhere the health and safety requirements, the radiation from the integrated antennas should present the least power absorbed per unit mass, which is quantified by the specific absorption rate (SAR). Second, to maintain easy wearing and reduce the discomfort when antennas are worn, they should be reasonably flexible, low profile, and conformal to the human body. Textile materials have been widely adopted in the wearable antenna design due to their light weight and flexibility properties [2]-[4]. However, fabrication tolerances are relatively large for antenna built using textile materials compared to those made using printed circuit board (PCB) machining [5]. Finally, the robustness of the wearable antenna performance against various types of structural deformations such as bending and crumpling should be guaranteed. Bearing in mind all the aforementioned issues, it becomes challenging to design an efficient miniaturized wearable antenna with a reliable performance.

In the literature, researchers have proposed several types of textile/flexible wearable antennas with different topologies. It was reported that the electromagnetic band gap (EBG) and artificial magnetic conductor (AMC) inspired antenna designs helped in minimizing the electromagnetic coupling to the human body compared to conventional antennas [4]-[6]. Table I compares antennas in terms of the resonance frequency, volume, antenna bandwidth, gain, and material type. These antennas are working within the industrial, scientific, and medical ISM 5.8 GHz band (5.725 GHz – 5.875 GHz). It is evident that the proposed textile antenna provides the largest antenna bandwidth that makes it less sensitive to the frequency detuning. Detuning may take place due to human body loading and/or structural deformation effects. In addition, the proposed antenna has a very small volume and provides a high gain. Similar observations are made when compared to flexible wearable antennas working within ISM 2.45 GHz band (2.4 GHz – 2.5 GHz) [7]-[9].

We proposed and experimentally realized a low-profile fully textile monopole antenna integrated with a compact AMC structure for wearable applications in the ISM 5.8 GHz band. In this paper, experimental and numerical results are presented. Measurements were performed to verify the

The paper was submitted December 2017. This work was supported by the Department of Electrical Engineering University of North Dakota and Rockwell Collins Corp.

A. Alemaryeen is with the Department of Electrical Engineering, University of North Dakota, Grand Forks, ND 58202-8382 USA. (e-mail: ala.alemaryeen@und.edu).

S. Noghanian is with the Department of Electrical Engineering, University of North Dakota, Grand Forks, ND 58202-8382 USA. (e-mail: sima.noghanian@und.edu).

This article has been accepted for publication in a future issue of this journal, but has not been fully edited. Content may change prior to final publication. Citation information: DOI 10.1109/TAP.2019.2902632, IEEE Transactions on Antennas and Propagation

TABLE I
COMPARISON OF THE PROPOSED ANTENNA WITH REPORTED WORK IN LITERATURE

Ref.	Year	Freq. (GHz)	Volume (mm^3)	B.W (GHz)	B.W (%)	Gain (dBi)	Material (dielectric/conductive)
[10]	2017	5.8	$2.84\lambda_0\times2.84\lambda_0\times0.15\lambda_0$	5.62 – 5.90	4.83	6.08	PDMS/NA
[4]	2016	5.4	$0.17\lambda_0\times0.17\lambda_0\times0.07\lambda_0$	5.15 – 5.87	13.0	NA	Felt/NA
[11]	2016	5.8	$1.74\lambda_0\times1.74\lambda_0\times0.13\lambda_0$	5.46 – 6.18	12.0	5.26	Felt/ShieldIt Super
[12]	2016	5.4	$2.94\lambda_0\times2.94\lambda_0\times0.12\lambda_0$	NA	6.70	7.25	Cotton/ NA
[13]	2015	5.8	$\pi\times(0.97\lambda_0)^2$ [area]$\times0.05\lambda_0$	5.56 – 6.03	8.10	3.83	Leather/Conductive Threads
[5]	2014	5.8	$1.93\lambda_0\times1.93\lambda_0\times0.05\lambda_0$	5.04 – 5.94	15.4	4.00	Felt/ShieldIt Super
[14]	2013	5.5	$0.74\lambda_0\times0.93\lambda_0\times0.04\lambda_0$	5.00 – 6.00	18.0	6.20	Photo Paper/Silver Ink
[15]	2012	5.5	$1.61\lambda_0\times1.42\lambda_0\times0.15\lambda_0$	5.04 – 6.04	18.1	5.00	Felt/ShieldIt Super
[16]	2012	5.5	$2.03\lambda_0\times2.03\lambda_0\times0.06\lambda_0$	NA	6.00	9.80	Jeans/ NA
[17]	2010	5.5	$1.80\lambda_0\times1.80\lambda_0\times0.13\lambda_0$	NA	12.4	5.20	Polyethylene Foam/Zelt
[6]	2009	5.8	$2.32\lambda_0\times2.32\lambda_0\times0.08\lambda_0$	5.40 – 6.15	12.0	5.20	Felt/Zelt
Proposed	2018	4.8	$1.70\lambda_0\times1.13\lambda_0\times0.06\lambda_0$	4.30 – 5.90	34.0	6.12	Pellon/Pure Copper Taffeta

expected antennas' performance and numerical investigations were carried out using CST Microwave Studio software (CST MWS) [18], including a single monopole and an AMC integrated antenna (AMC antenna). In section II we present the design methodology and characterization of the monopole antenna and AMC structure. In section III, performance analysis of the proposed antenna system in free-space condition, in both flat form and under deformation effects (bending and crumpling conditions) is presented. Influence of on-body operation on the AMC antenna is investigated and compared with the monopole antenna in section IV. Three different body models, of different compositions and shapes, were used to characterize antennas' performance for different on-body deployment scenarios. In addition, a series of numerical simulations for SAR analysis, as well as on-body phantom validation that were carried out are discussed in this section. Section V draws the conclusion.

II. ANTENNA TOPOLOGY AND MATERIALS

The proposed topology consists of a coplanar waveguide (CPW) fed monopole antenna with dimensions of 27 × 34 mm^2. The monopole antenna is placed on an AMC layer of 4 × 6 units, with overall dimensions of 102 × 68 mm^2. These structures are designed on a 1.8 *mm*-thick Pellon fabric substrate, with a relative permittivity (ε_r) and loss tangent (tanδ) of 1.08 and 0.008, respectively. A 0.08 *mm*-thick electro-textile, Pure Copper Taffeta from LessEMF [19], is used to fabricate the conductive layers. Its estimated conductivity is 2.5×10^5 S/m. Geometries of the monopole antenna and AMC unit cell are based on the proposed designs in [20]-[21], respectively. By tuning the geometrical dimensions of both monopole antenna and AMC unit cell, the desired impedance matching and radiation properties of the AMC antenna are achieved in the operation ISM 5.8 GHz band. The optimized dimensions of monopole antenna and AMC unit cell are presented in Figs. 1(a) and 2(a), respectively. It is worth mentioning that in the design and simulation phase, the AMC array was increased by one row and one column at a time until a satisfactory performance in terms of high gain, high front-to-back-ratio (FBR), and good impedance matching was achieved within ISM 5.8 GHz frequency band. In this process the tradeoff between the antenna size and performance was considered.

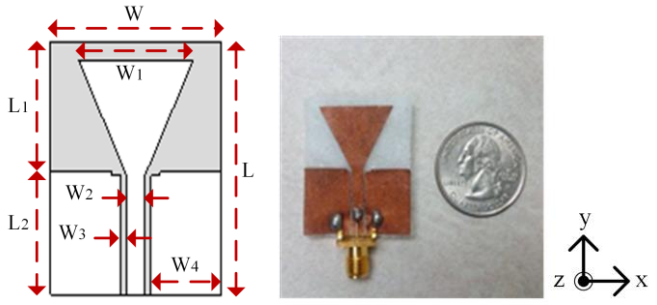

(a) (b)

Fig. 1. (a) Configuration of CPW-fed monopole antenna and (b) a photograph of the fabricated monopole prototype. The optimized dimensions in *mm* are W = 27, L = 34, L_1 = 15.5, L_2 = 16.5, W_1 = 19, W_2 = 3, W_3 = 0.4, and W_4 = 11.6.

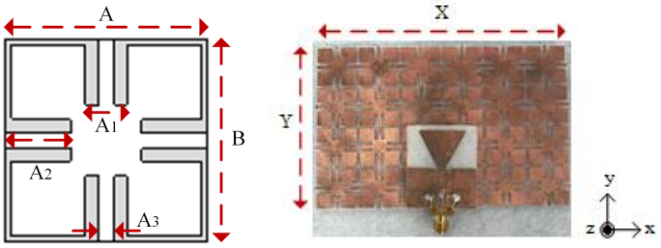

(a) (b)

Fig. 2. (a) Configuration of AMC unit cell and (b) a photograph of the fabricated AMC antenna prototype. The optimized dimensions in *mm* are A = 17, B = 17, A_1 = 3.5, A_2 = 5.5, A_3 = 1.3, X = 102, and Y = 68.

Fabrication process was performed using Silhouette® cutting machine and simple dimensioning tools. Prototypes of fabricated monopole antenna and AMC reflector are shown in Figs. 1(b) and 2(b), respectively. Reflection phase characterization method was used to analyze the AMC structure. In the proposed AMC unit cell, the exact zero-reflection phase point is at 5.8 GHz. The achieved bandwidth within ±90° phase values is 390 MHz (5.61 GHz – 6.00 GHz).

III. ANTENNA PERFORMANCE IN FREE SPACE

A. Antenna Performance in Planar Configuration

Reflection coefficients (S_{11}) of the proposed antenna measured in free-space, without, and with AMC reflector, named as "*monopole*" and "*AMC*" antennas, respectively, are depicted in Fig. 3. S_{11} measurements were carried out using Keysight E5071C vector network analyzer (300 kHz – 20 GHz frequency operating range). The inclusion of the AMC reflector resulted in a shift in the resonance frequency (f_r) from

This article has been accepted for publication in a future issue of this journal, but has not been fully edited. Content may change prior to final publication. Citation information: DOI 10.1109/TAP.2019.2902632, IEEE Transactions on Antennas and Propagation

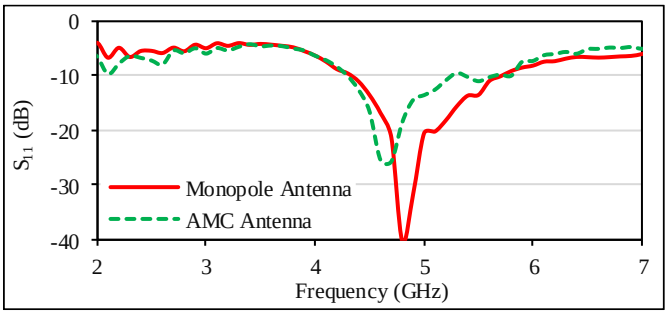

Fig. 3. Measured S_{11} of monopole and AMC antennas in free-space.

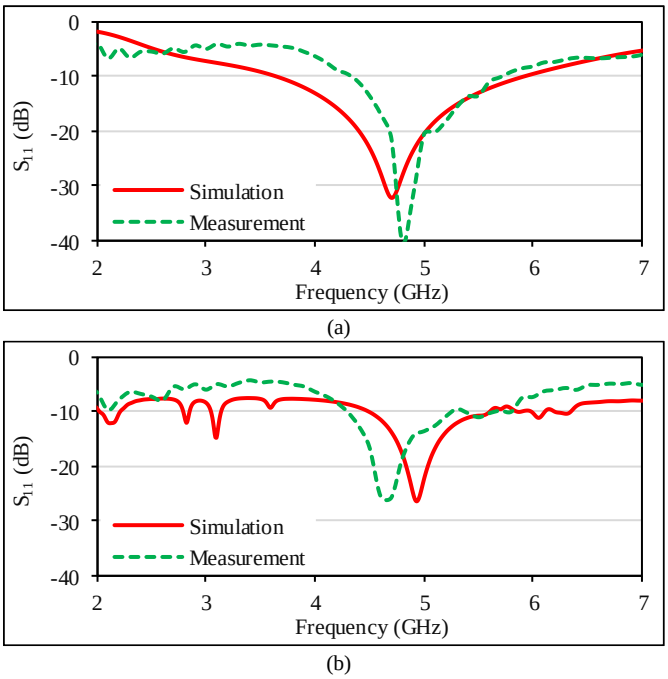

Fig. 4. Simulated and measured S_{11} of (a) monopole and (b) AMC antennas in free-space.

4.8 GHz (monopole antenna) to 4.7 GHz (AMC antenna) with a 14.47 dB increase in the S_{11} level. On the other hand, a robust impedance bandwidth (4.3 GHz – 5.9 GHz) is achieved in both cases.

As shown in Fig. 4, simulated and measured S_{11} are compared for both antennas. In case of monopole antenna, simulated impedance bandwidth of (3.60 GHz – 5.95 GHz) is found to be wider than the measured bandwidth of (4.3 GHz – 5.9 GHz). On the other hand, compared to simulation results, a shift in the measured operating impedance bandwidth of 200 MHz toward lower frequencies is observed in case of AMC antenna. However, both antennas cover the entire ISM 5.8 GHz band (5.725 GHz – 5.875 GHz). It's worth mentioning that difficulties were encountered during the fabrication and testing processes of textile antennas. Elastic properties of textile materials, where the variation of dimensions due to stretching and compression are typical for fabrics, can be a major source of inaccuracies. This dimension changes could lead to changes in the resonant length of the antenna and detune its frequency band. For example, the dielectric substrate height for monopole antenna was considered to be 1.8 *mm* in the simulation. However, when fabricated, the

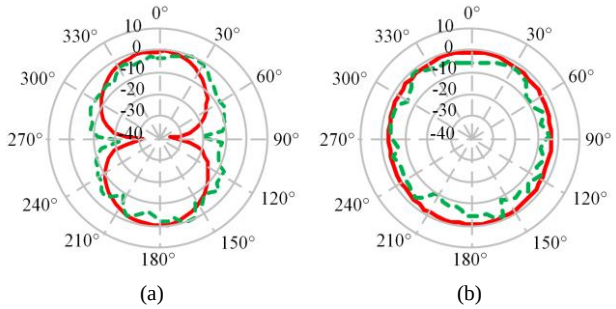

Fig. 5. Simulated (solid) and measured (dashed) co-pol radiation of monopole antenna at 5.8 GHz in (a) E-plane and (b) H-plane.

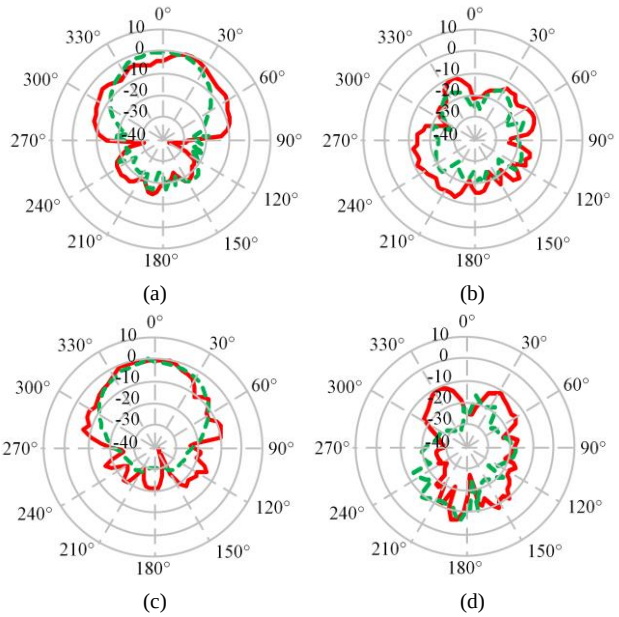

Fig. 6. Simulated (dashed) and measured (solid) (a) co-pol radiation in E-plane, (b) cross-pol radiation in E-plane, (c) co-pol radiation in H-plane, and (d) cross-pol radiation in H-plane of AMC antenna at 5.8 GHz.

Pellon fabric did not give the constant thickness. The thickness of the fabric may change at different parts. In addition, during fabrication, when the electro-textile material is cut into the shape of the patch, a simple cutting machine and scissor were used. The manual cutting does not provide very clean straight edges and some threads might be fringed. Keeping the constant spacing between patch surface and the AMC layer, and cutting precise and straight edges of the conductive elements was very challenging when fabricating textile antennas manually. For a better result a laser cutting method can be utilized, but the authors did not have access to laser cutting tools.

The normalized far-field radiation patterns of the principal planes, E-plane (*yz*-plane) and H-plane (*xz*-plane), were measured inside the University of North Dakota anechoic chamber with an automated antenna movement platform. Radiation patterns of monopole and AMC antennas at 5.8 GHz are depicted in Figs. 5 and 6, respectively. The measured radiation patterns in both planes as well as gain values agree well with the simulated results, for both antennas. The monopole antenna retains a dipole like pattern in its E-plane and an omni-directional pattern in its H-plane. In both planes, the measured and simulated cross-polarization radiation levels are below -20 dB. Addition of the AMC resulted in a quasi-

hemispherical radiation pattern. The increase in the FBR was achieved by the in-phase reflection property of the AMC structure. This minimizes the SAR value and makes the antenna more robust and less sensitive to the loading effects of the human body. The measured gain for the proposed AMC antenna is 6.12 dBi compared to 2.65 dBi for the monopole antenna. The simulated gains were 7.34 dBi and 3.18 dBi for AMC and monopole antennas, respectively.

B. Antenna Performance under Structural Deformation Effects

In a practical on-body application, the textile antenna may change its shape and dimensions due to conformability with the surface of the human body. Therefore, it is essential to study the performance of the antenna under structural deformation conditions such as bending and crumpling. In such conditions, f_r and S_{11} need to be evaluated since they are prone to change due to impedance mismatch and change in the effective electrical length of the radiating element [8].

For bending analysis, the AMC antenna was placed on a foam cylinder with a radius of 50 *mm*. This radius was carefully chosen to emulate the antenna conformed on an average human arm. AMC antenna bending is studied for two bending configurations, i.e. antenna bending in the E-plane (around *y*-axis) and the H-plane (around *x*-axis). Fig. 7 shows S_{11} simulation and measurement results in both bending directions. Despite our best effort, some discrepancies between simulations and measurements, particularly in case of E-plane bending, exists. This may be due to fabrication inaccuracy discussed earlier, as well as the antenna misalignments, which are unavoidable, since it is impossible to reach an ideal uniformity of the bending radius across the antenna structure as accurate as in simulations [22]. Bending AMC antenna in the H-plane direction caused a slight resonance frequency shift, of order of 10 MHz, to a higher frequency within frequency band of interest. On the other hand, more stable resonance frequency is observed in case of E-plane bending. Both bent antennas retained their impedance bandwidth as achieved in the flat AMC antenna. Variations in the radiation characteristics of the AMC antenna due to bending conditions at 5.8 GHz are summarized in Table I. These results are based on simulation, and they show that antenna's radiation characteristics are sensitive to both E- and H-plane bending, causing reduction in the antenna gain and FBR.

For crumpling analysis, the crumpling profile was defined by the crumple depth (*N*) and the peak distance between the two troughs (*M*). In this study, *N* was chosen to be 6 *mm* and *M* was chosen 31 *mm* and 24 *mm*, for crumpling cases 1 and 2, respectively, as shown in Fig. 8(a). The crumpling profiles were made by using foam backing (Fig. 8(a)). In measurements, the AMC antenna was crumpled in the H-plane direction (along *x*- axis). Measured S_{11} for the crumpling cases are depicted in Fig. 8(b). A shift in the resonance frequency was observed. In addition, a wider impedance bandwidth existed with a good impedance matching within the frequency band of interest.

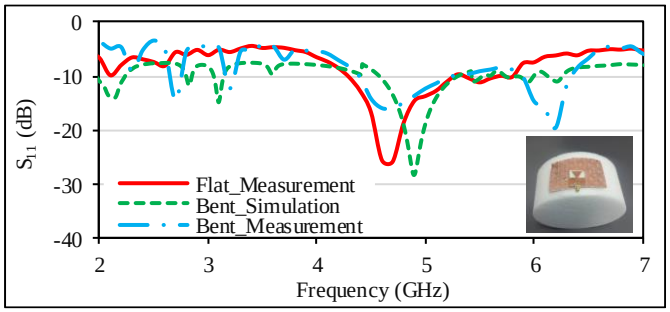

(a)

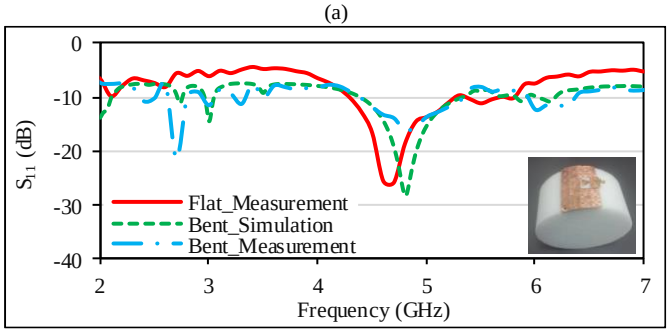

(b)

Fig. 7. S_{11} results of AMC antenna in free-space; (a) E-plane bending and (b) H-plane bending.

TABLE I
RADIATION CHARACTERISTICS SUMMARY OF AMC ANTENNA AT 5.8 GHZ

Scenario	Gain (dBi)	HPBW[a]: E-plane	HPBW: H-plane	FBR[b]
Flat	7.34	48.50	28.60	27.57
E-plane bending	4.05	45.10	40.30	19.40
H-plane bending	5.40	56.60	31.00	18.83

[a]HPBW given in degrees and [b]FBR given in dB.

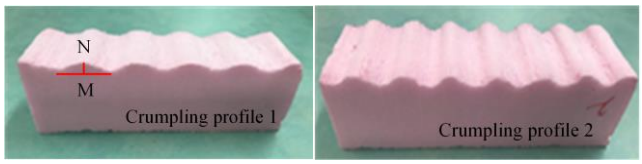

(a)

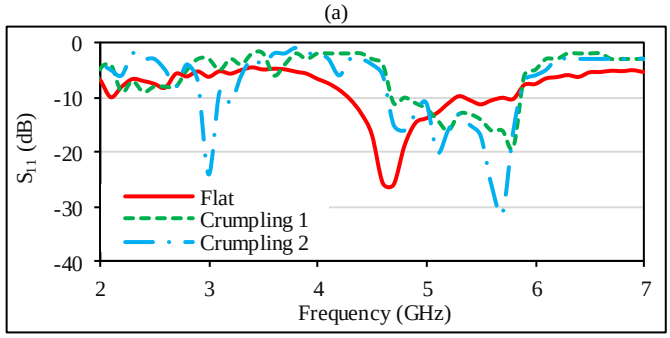

(b)

Fig. 8. (a) Photograph depicting crumpling profiles and (b) S_{11} measurement results of crumpled AMC antenna in free-space.

IV. ANTENNA PERFORMANCE ON BODY

To validate the on-body performance and investigate effects of human body loading on the proposed antennas, we performed full-wave simulations using monopole and AMC antennas in the vicinity of three different human body models. First, we used a body model of averaged human arm phantom properties of ε_r = 21.2 and σ = 3.38 S/m, at 5.8 GHz [23]. Second, a multilayer human tissue model was employed to

This article has been accepted for publication in a future issue of this journal, but has not been fully edited. Content may change prior to final publication. Citation information: DOI 10.1109/TAP.2019.2902632, IEEE Transactions on Antennas and Propagation

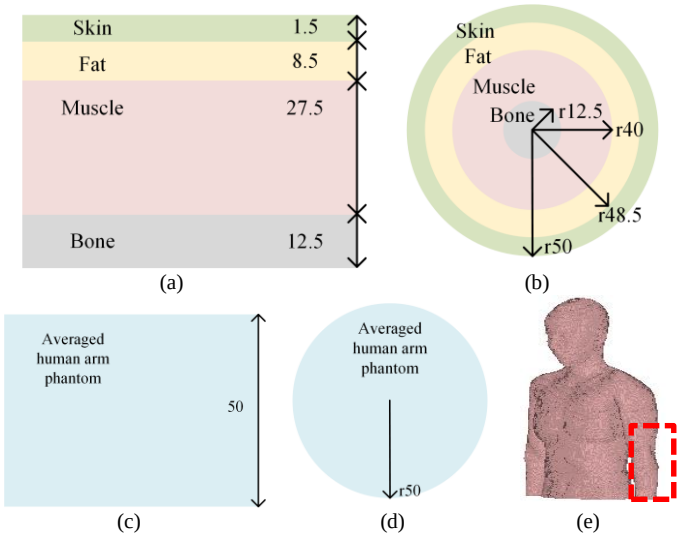

Fig. 9. Cross-sections of simulated human tissue models (dimensions are in *mm*); (a) BM_layered (cubic model), (b) BM_layered (cylindrical model), (c) BM_equivelent (cubic model), (d) BM_equivalent (cylindrical model), and (e) Ella model.

mimic the human arm. This model consists of four layers representing skin, fat, muscle, and bone tissues. Properties of dispersive tissue layers were obtained from the material library in CST MWS. Finally, the proposed antennas were placed on the arm of Ella model, which represents a 26 year old female with the height of 1.36 m and weight of 57.3 kg belonging to the Virtual Family [24]. These body models are named "*BM_equivalent*", "*BM_layered*", and "*Ella*", respectively. Since the antennas can be bent and worn on the user's arm, their performance on the proposed human body models are studied under two bending configurations, in addition to the flat one: bending in the E- and H-planes.

For this purpose, we designed BM_equivalent and BM_layered body models in cubic and cylindrical forms, respectively. The total size of the cubic tissue body model is 177.2 × 177.2 × 50 mm^3 (length × width × depth), which is equivalent in volume to the cylindrical tissue body model that has 200 *mm* height and 50 *mm* radius. The numerical setups for the different human body models are shown in Fig. 9. The same cylindrical topology was used when antennas were bent around Ella's arm, as shown in Fig. 9(e). To reduce the simulation time, a reasonably sized portion of Ella's arm (sectional area of about the same size as other models) was selected for simulation, instead of simulating the antenna on the entire numerical body model. In all the studied scenarios, antennas were assumed to be separated from the skin layer by an additional layer of Pellon fabric of 1.8 *mm* thickness to account for clothing. SAR performance evaluation analysis was carried out. Also, antenna's performance on a realistic muscle tissue phantom was measured.

A. Antenna Performance in Planar Configuration

A comparison between antennas' performances, i.e. monopole and AMC antennas, in free-space and on the body models, while antennas were in flat form, are presented in this subsection. Simulation results for S_{11} are shown in Fig. 10. In the case of monopole antenna, similar loading effects due to

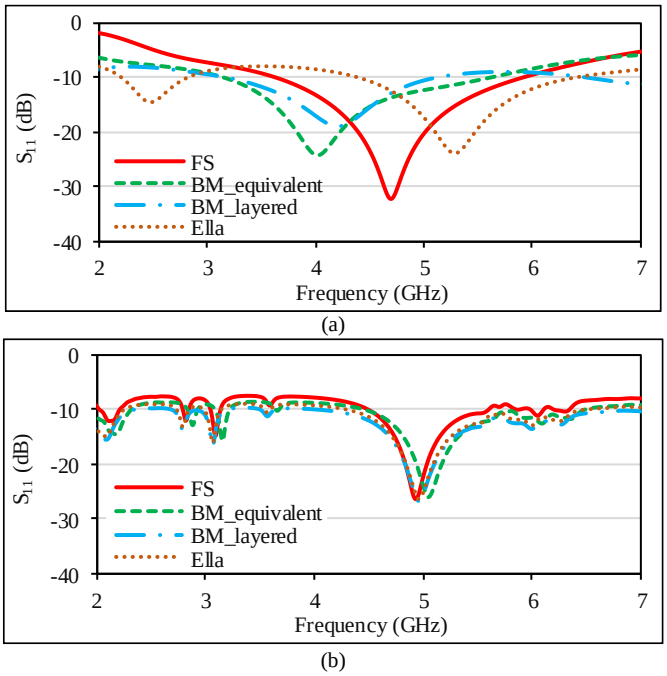

Fig. 10. S_{11} simulation results of flat antennas in free-space (FS), equivalent human body model (BM_equivalent), layered human body model (BM_layered), and Ella model for (a) monopole and (b) AMC antennas.

different human body models are observed. These effects are frequency detuning toward lower frequencies, and a reduction in the -10 dB impedance bandwidth, compared to the free-space case. The detuning of frequency is due to the high dielectric constant values of various tissues that were considered in the human body models. The maximum shift in the resonant frequency is observed in the case of BM_equivalent body model, from 4.7 GHz (in free-space) to 4.10 GHz (on body). While the maximum bandwidth reduction is observed in the case of BM_layered body model from the bandwidth of 3.60 GHz – 5.95 GHz (in free-space), to the bandwidth of 3.18 GHz – 5.10 GHz (on body).

On the other hand, as shown in Fig. 10(b), AMC antenna showed a robust impedance matching characteristics, compared to monopole antenna. However, a slight bandwidth broadening was observed, when it was placed on Ella body model. Radiation characteristics summary, i.e., antenna gain, HPBW, and FBR are given in Table II at 5.8 GHz. For monopole antenna, placing antenna on different human body models caused an improvement in the antenna gain and FBR, and a reduction in the HPBW. In contrast, with the presence of AMC structure stable results and improvement in the FBR can be observed.

B. Antenna Performance in Bending Configuration

For comparison purposes, results of antennas bending in free-space condition are presented to examine the impact of human body loading on the bent antennas. S_{11} results are shown in Figs. 11 and 12 for monopole and AMC antennas, respectively. In general, the impact of human body loading on the bent monopole antenna, in both directions, is similar. A shift in the resonant frequency toward higher values, as well as a reduction in the impedance bandwidth are observed.

This article has been accepted for publication in a future issue of this journal, but has not been fully edited. Content may change prior to final publication. Citation information: DOI 10.1109/TAP.2019.2902632, IEEE Transactions on Antennas and Propagation

TABLE II
RADIATION CHARACTERISTICS SUMMARY FOR FLAT ANTENNAS AT 5.8 GHZ

Scenario	Gain (dBi)	HPBW[a]: E-plane	HPBW: H-plane	FBR[b]
Monopole Antenna				
FS[c]	3.18	54.10	165.60	12.70
BM_equivalent[d]	5.00	44.00	89.30	29.05
BM_layered[e]	5.85	42.40	71.50	36.94
Ella	6.05	50.20	85.50	33.53
AMC Antenna				
FS	7.34	48.50	28.60	27.57
BM_equivalent	8.29	45.90	25.30	44.88
BM_layered	8.15	45.30	24.70	41.39
Ella	7.89	44.78	23.65	26.86

[a]HPBW given in degrees, [b]FBR given in dB, [c]Free Space (FS), [d]Equivalent human body model (BM_equivalent), and [e]Layered human body model (BM_layered).

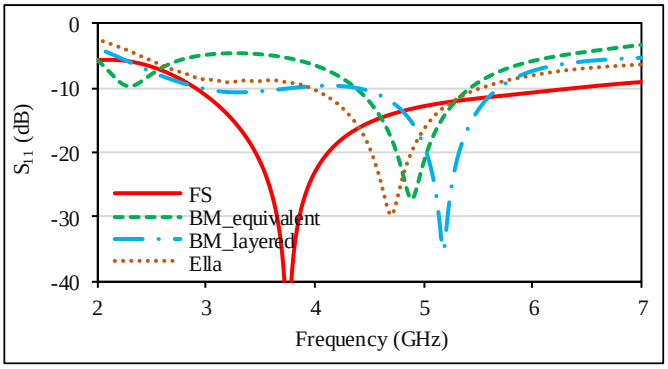

(a)

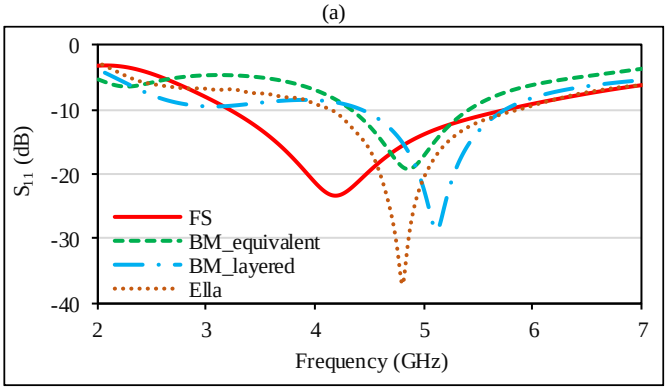

(b)

Fig. 11. Simulation results of bent monopole antenna in free space (FS), equivalent human body model (BM_equivalent), layered human body model (BM_laered), and Ella model in (a) E-plane and (b) H-plane.

The monopole antenna is prone to bending. On the contrary, with the presence of AMC structure, the antenna retains its impedance matching properties with a slight detuning of the resonant frequency. Therefore, AMC provides a good insolation layer. Radiation characteristics of monopole and AMC antenna for all the studied bending configurations are summarized in Tables III at 5.8 GHz. In the case of monopole antenna, the presence of different body models resulted in improvement in the antenna gain and FBR and reduction in the HPBW. On the other hand, stable results with improvement in the FBR are observed in case of AMC antenna.

C. SAR Validation

The SAR level of wearable antenna must be validated in the antenna design stage to ensure conformance to safety regulations. Moreover, SAR is utilized in order to address the health risks imposed by wearable antennas to the human body. Hence, the radiofrequency energy absorbed by human tissues should not exceed critical values of 1.6W/kg for any 1 g tissue or 2W/kg for any 10 g tissue according to the guidelines of the IEEE C95.1-1999 [25] and the IEEE C95.1-2005 standards [26], respectively. SAR is calculated based on the root mean

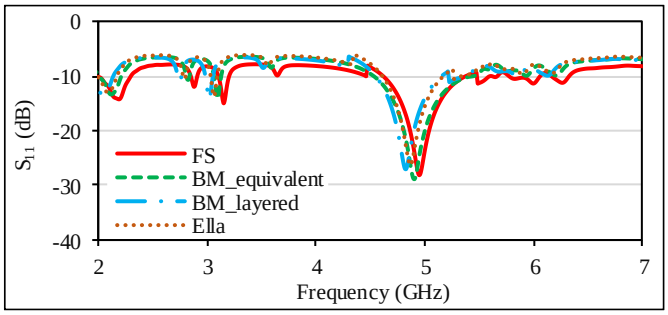

(a)

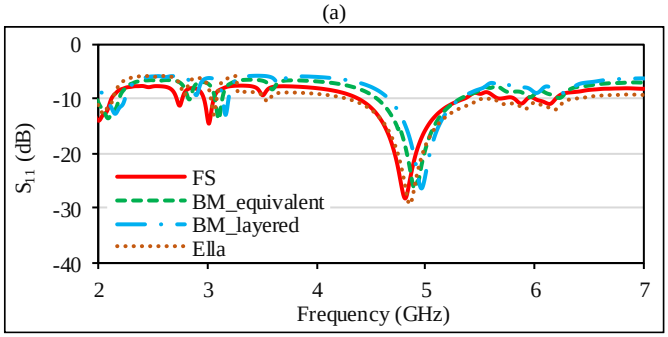

(b)

Fig. 12. Simulation results of bent AMC antenna in free-space (FS), equivalent human body model (BM_equivalent), layered human body model (BM_layered), and Ella model in (a) E-plane and (b) H-plane.

TABLE III
RADIATION CHARACTERISTICS SUMMARY FOR BENT MONOPOLE ANTENNA

Scenario	Gain (dBi)	HPBW[a]: E-plane	HPBW: H-plane	FBR[b]
Monopole Bending in E-plane				
FS[c]	2.98	55.50	146.4	5.66
BM_equivalent[d]	3.81	45.20	108.20	26.13
BM_layered[e]	4.69	43.40	91.00	37.26
Ella	3.98	40.32	96.36	29.68
Monopole Bending in H-plane				
FS	3.90	53.20	134.6	5.81
BM_equivalent	4.33	44.30	82.30	35.66
BM_layered	4.90	48.50	83.80	22.16
Ella	4.89	43.36	93.96	10.46
AMC Bending in E-plane				
FS	4.05	45.10	40.30	19.40
BM_equivalent	4.39	48.00	40.40	21.68
BM_layered	4.22	43.50	40.50	21.66
Ella	4.36	30.96	39.90	20.36
AMC Bending in H-plane				
FS	5.40	56.60	31.00	18.83
BM_equivalent	5.29	52.00	29.70	33.82
BM_layered	6.29	53.50	29.70	25.20
Ella	5.96	53.97	28.64	17.68

[a]HPBW given in degrees, [b]FBR given in dB, [c]Free Space (FS), [d]Equivalent human body model (BM_equivalent), and [e]Layered human body model (BM_layered).

This article has been accepted for publication in a future issue of this journal, but has not been fully edited. Content may change prior to final publication. Citation information: DOI 10.1109/TAP.2019.2902632, IEEE Transactions on Antennas and Propagation

square (rms) of the electric field strength inside the human body and the human body tissue properties such as conductivity and mass density [27]. Researchers have been using the numerical evaluation of SAR as the mean of design validation due to the equipment scarcity and costs involved in experimentally evaluated SAR. In the area of textile antennas, such simulations have been shown to agree well with measurements [28].

In this work, a series of numerical SAR investigations based on mass-averaged method were performed using IEEE C95.1 standard provided in the CST MWS software. The input power to the antennas for SAR calculations was set at 1 W (rms). The calculated SAR results are summarized in Tables IV for monopole and AMC antennas located on different body models in flat form and under different bending conditions. For 10 g SAR analysis, despite the use of three different body models of different tissue composition, the obtained SAR values of the proposed antennas (individually) in flat form and under bending effects are comparable. This suggests that for the proposed antennas; 10 g SAR analysis is less sensitive to antenna deformation and shape and body tissue composition. Same discussion can be applied to 1 g SAR analysis of monopole antenna. On the other hand, in case of AMC antenna, 1 g SAR values showed sensitivity to bending conditions. The minimum 1 g SAR value of 0.37 W/Kg is achieved due to AMC antenna E-plane bending on Ella model and the maximum value is observed due to AMC antenna H-plane bending on Ella model. Most importantly, all evaluated SAR values for the AMC antenna are far below the regulated SAR thresholds, while thisdoes not happen for the monopole antenna. The reason lies in the fact that monopole antenna provides an omnidirectional pattern while the AMC antenna has a directive radiation characteristic. The SAR analysis is demonstrating the superiority of the AMC antenna for operation in close proximity to the human body. Thus, it can be concluded that maintaining the SAR values within the regulated levels will not be an issue for future applications of the proposed AMC antenna.

D. Experimental Analysis of Antenna Performance on Body Phantom

In order to get an initial insight into the human body loading effects in a scenario of realistic operation, the fabricated antennas were placed on the top of muscle tissue phantom. A cylindrical container of 45 *mm* radius and 25 *mm* length was filled with the muscle tissue phantom. The details of phantom preparation can be found in [29]. The dielectric constant and loss tangent of muscle tissue phantom were measured using Keysight 85070E high-performance dielectric probe, for frequency range of 1 GHz – 6 GHz, as shown in Fig. 13. As can be seen in Fig. 14, the presence of muscle phantom leads to a 400 MHz shift in the resonant frequency toward a higher value, in addition to about 25 dB increase in the S_{11} level, for the monopole antenna. On the other hand, in the presence of the AMC reflector, the antenna is able to maintain a good impedance matching when positioned on muscle tissue phantom.

TABLE IV
SAR ANALYSIS SUMMARY OF ANTENNAS AT 5.8 GHZ

Scenario	1 g Tissue (W/Kg)	10 g Tissue (W/Kg)
Flat Monopole Antenna		
BM_equivalent[a]	47.26	12.59
BM_layered[b]	48.59	11.90
Ella	45.97	13.19
Monopole Antenna Bent in E-plane		
BM_equivalent[a]	49.05	11.32
BM_layered[b]	48.61	10.56
Ella	46.23	12.35
Monopole Antenna Bent in H-plane		
BM_equivalent[a]	45.42	14.17
BM_layered[b]	47.88	11.60
Ella	48.32	11.89
Flat AMC Antenna		
BM_equivalent[a]	0.60	1.18
BM_layered[b]	0.61	1.49
Ella	0.56	1.18
AMC Antenna Bent in E-plane		
BM_equivalent[a]	0.59	1.64
BM_layered[b]	0.37	1.76
Ella	0.53	1.54
AMC Antenna Bent in H-plane		
BM_equivalent[a]	0.93	1.77
BM_layered[b]	0.88	1.40
Ella	0.97	1.32

[a]Equivalent human body model (BM_equivalent), and [b]Layered human body model (BM_layered).

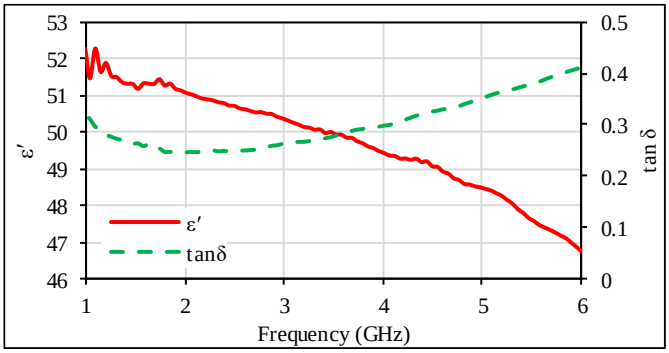

Fig. 13. Muscle phantom dielectric property measurements; permittivity (ε′) and loss tangent (tan δ).

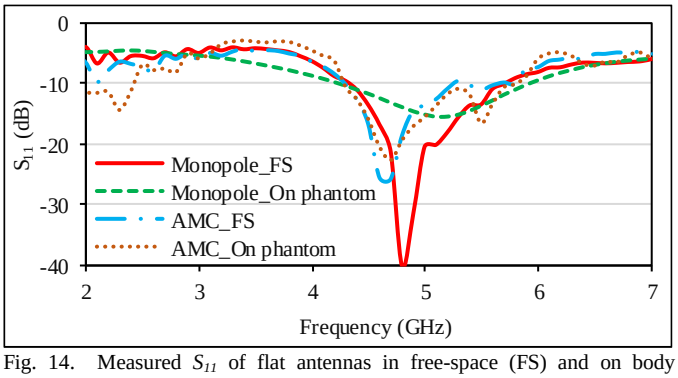

Fig. 14. Measured S_{11} of flat antennas in free-space (FS) and on body phantom (On phantom).

V. CONCLUSION

In this paper, we have proposed a compact conformal textile AMC antenna for wearable applications. The antenna design methodology and fabrication process were summarized and presented. In order to verify the simulation results, prototypes of the antennas were fabricated and measured in different

conditions. In free-space, the realized AMC antenna showed an impedance bandwidth of 34% (4.30 GHz – 5.90 GHz), with a gain value of 6.12 dBi. Numerical simulations and experimental measurements have further revealed that the proposed AMC antenna is robust in respect to impedance resonance frequency, showing minimal changes due to structural deformation such as bending and crumpling, as well as loading effects of human body. In addition, the inclusion of the AMC reflector considerably reduces the SAR values and the back radiation, making the AMC antenna far superior to a single monopole antenna.

ACKNOWLEDGEMENTS

The authors would like to acknowledge the assistance of Professors Yi-hsiang Chang, Satish Sharma and Fazel-Rezai and Mr. Qusay Al-Kaseasbeh in different steps of antenna fabrication and testing. Rockwell Collins Inc. is acknowledged for its financial support.

REFERENCES

[1] S. Yan, P. J. Soh, and G. A. E. Vandenbosch, "Made to be worn," *Electron. Lett.*, vol. 50, no. 6, p. 420, 2014.
[2] S. Yan and G. A. E. Vandenbosch, "Radiation pattern-reconfigurable wearable antenna based on metamaterial structure," *IEEE Antennas Wirel. Propag. Lett.*, vol. 15, pp. 1715–1718, 2016.
[3] A. Alemaryeen and S. Noghanian, "Performance analysis of textile AMC antenna on body model," in *Proc. IEEE AP-S Int. Symp*, 2017, pp. 41–42.
[4] S. Collardey, M. Mantash, K. Mahdjoubi, and A.-C. Tarot, "Design methodology for wearable antenna on artificial magnetic conductor using stretch conductive fabric," *Electron. Lett.*, vol. 52, no. 2, pp. 95–96, 2016.
[5] S. Yan, P. J. Soh, and G. A. E. Vandenbosch, "Low-profile dual-band textile antenna with artificial magnetic conductor plane," *IEEE Trans. Antennas Propag.*, vol. 62, no. 12, pp. 6487–6490, 2014.
[6] S. Zhu and R. Langley, "Dual-band wearable textile antenna on an EBG substrate," *IEEE Trans. Antennas Propag.*, vol. 57, no. 4 PART. 1, pp. 926–935, 2009.
[7] S. Velan, E. F. Sundarsingh, M. Kanagasabai, A. K. Sarma, C. Raviteja, R. Sivasamy, and J. K. Pakkathillam, "Dual-band EBG integrated monopole antenna deploying fractal geometry for wearable applications," *IEEE Antennas Wirel. Propag. Lett.*, vol. 14, pp. 249–252, 2015.
[8] H. R. Raad, A. I. Abbosh, H. M. Al-Rizzo, and D. G. Rucker, "Flexible and compact AMC based antenna for telemedicine applications," *IEEE Trans. Antennas Propag.*, vol. 61, no. 2, pp. 524–531, 2013.
[9] B. S. Abirami and E. F. Sundarsingh, "EBG-backed flexible printed Yagi-Uda antenna for on-body communication," *IEEE Trans. Antennas Propag.*, vol. 65, no. 7, pp. 3762–3765, 2017.
[10] M. N. Ramli, P. J. Soh, M. F. Jamlos, H. Lago, N. M. Aziz, and A. A. Al-Hadi, "Dual-band wearable fluidic antenna with metasurface embedded in a PDMS substrate," *Appl. Phys. A Mater. Sci. Process.*, vol. 123, no. 2, 2017.
[11] P. J. Soh, F. N. Giman, M. F. Jamlos, H. Lago, and A. A. Al-Hadi, "A C-slotted dual band textile antenna for WBAN applications," in *URSI Asia-Pacific Radio Science Conference*, 2016, pp. 1621–1624.
[12] A. Ahmad, F. Faisal, S. Khan, S. Ullah, and U. Ali, "Performance analysis of a wearable and dual band planar antenna using a mushroom-like electromagentic bandgap (EBG) ground plane," in *International Conference on Open Source Systems and Technologies (ICOSST)*, 2016, pp. 24–29.
[13] Y. Hong, J. Choi, and J. Tak, "Textile antenna with EBG structure for body surface wave enhancement," *Electron. Lett.*, vol. 51, no. 15, pp. 1131–1132, 2015.
[14] B. S. Cook and A. Shamim, "Utilizing wideband AMC structures for high-gain inkjet-printed antennas on lossy paper substrate," *IEEE Antennas Wirel. Propag. Lett.*, vol. 12, pp. 76–79, 2013.
[15] M. Mantash, A. C. Tarot, S. Collardey, and K. Mahdjoubi, "Investigation of flexible textile antennas and AMC reflectors," *Int. J. Antennas Propag.*, vol. 2012, 2012.
[16] S. Tarigonda and B. Bharath, "Design and fabrication of dual-band coplanar antenna using EBG structures," in *International Conference on Computing Sciences (ICCS)*, 2012, pp. 249–254.
[17] N. Chahat, M. Zhadobov, R. Sauleau, and K. Mahdjoubi, "Improvement of the on-body performance of a dual-band textile antenna using an EBG structure," in *Loughborough Antennas and Propagation Conference (LAPC)*, 2010, pp. 465–468.
[18] CST Microwave Studio [Online]. Available: http/www.cst.com. [Accessed: August, 2016].
[19] LessEMF [Online]. Available: http://www.lessemf.com. [Accessed: August, 2016].
[20] W. Liu and P. Kao, "CPW-fed triangular monopole antenna for ultra-wideband operation," *Microw. Opt. Technol. Lett.*, vol. 47, no. 6, pp. 580–582, 2005.
[21] J. R. J. Sohn, H.-S. H. Tae, J.-G. J. J.-H. Lee, and J.-G. J. J.-H. Lee, "Comparative analysis of four types of high-impedance surfaces for low profile antenna applications," in *AP-S IEEE Int. Symp. (Digest) Antennas Propag. Society*, 2005, vol. 1A, pp. 758–761.
[22] H. M. R. Nurul, P. J. Soh, M. F. A. Malek, and G. A. E. Vandenbosch, "Dual-band suspended-plate wearable textile antenna," *IEEE Antennas Wirel. Propag. Lett.*, vol. 12, pp. 583–586, 2013.
[23] CTIA Certification Standard, "Test Plan for Wireless Device Over-the-Air Performace" Revosion 3.5.2, September 2015.
[24] M.-C. Gosselin, E. Neufeld, H. Moser, E. Huber, S. Farcito, L. Gerber, M. Jedensjö, I. Hilber, F. Di Gennaro, B. Lloyd, E. Cherubini, D. Szczerba, W. Kainz, and N. Kuster, "Development of a new generation of high-resolution anatomical models for medical device evaluation: the Virtual Population 3.0.," *Phys. Med. Biol.*, vol. 59, no. 18, pp. 5287–5303, 2014.
[25] IEEE Std C95.3-2002: "IEEE recommended practice for measurements and computations of radio frequency electromagnetic fields with respect to human exposure to such fields, 100 kHz–300 GHz", 2002.
[26] Commission of European Communities., "Council recommendation on limits for exposure of the federal public to electromagnetic fields: 0Hz-300 GHz", 1998.
[27] S. Yan, P. Jack Soh, and G. A. E. Vandenbosch, "Compact all-textile dual-band antenna loaded with metamaterial-inspired structure," *IEEE Antennas Wirel. Propag. Lett.*, vol. 14, pp. 1486–1489, 2015.
[28] P. J. Soh, G. A. E. Vandenbosch, F. H. Wee, A. Van Den Bosch, M. Martinez-Vazquez, and D. M. M. P. Schreurs, "Specific absorption rate (SAR) evaluation of biomedical telemetry textile antennas," in *IEEE MTT-S International Microwave Symposium Digest*, 2013, pp. 1–3.
[29] T. Yilmaz, R. Foster, and Y. Hao, "Broadband tissue mimicking phantoms and a patch resonator for evaluating noninvasive monitoring of blood glucose levels," *IEEE Trans. Antennas Propag.*, vol. 62, no. 6, pp. 3064–3075, 2014.

Ala Alemaryeen earned a B.Sc. degree in electrical engineering from Mutah University, Jordan, in 2012, and a M.Sc. in electrical engineering from University of North Dakota (UND), USA, in 2015. She is currently working towards a Ph.D. degree in electrical engineering at UND. Her current research interests include antenna theory, wearable and implantable antennas, electromagnetics, and wireless communications.

Sima Noghanian earned M.Sc. and Ph.D. degrees, both in electrical engineering, from the University of Manitoba, Winnipeg, Canada, in 1996 and 2001, respectively. She was an Assistant Professor in the Department of Electrical Engineering, Sharif University of Technology, Iran, during 2002-2003. From 2003 to 2008, she was an Assistant Professor in the Department of Electrical and Computer Engineering, University of Manitoba, Canada. She has been currently an Associate Professor of the Department of Electrical Engineering, University of North Dakota, USA since 2008. She is currently a visiting professor at San Diego State University. Her research interests include antenna design and modeling, flexible and wearable antennas, wireless power transfer, and microwave imaging. Dr. Noghanian is currently an associate editor for IEEE Antennas and Wireless Propagation Letters, IEEE Antenna Magazine, The Applied Computation Electromagnetics Journal, and AEU - International Journal of Electronics and Communications.